FACULTY OF ENGINEERING, COMPUTING AND THE ENVIRONMENT

School of *Computer Science and Mathematics*

MSc DEGREE
IN
Data Science

Sasindu Mihiran Piyarathna

K2453742

Reconstructing Low Radiation CT Scans using Transformer and UNet Res Based Neural Networks

Experiment-based Project

18.09.2025

Professor Jamshid Dehmeshki

Kingston University London

Reconstructing Low Radiation CT Scans using Transformer and UNet Res Based Neural Networks

Sasindu Mihiran Piyarathna

CI7000 - Project Dissertation

{k2453742}

***Abstract* - Computed tomography from low radiation dose is challenging due to the high noise and artefacts from the projection data. The problem escapes the domain of linear algorithms due to the complexity of noise and the high bar of structural similarity expected in the reconstruction to feasibly make medical diagnosis. Popular NN based attempts include complex and very computationally costly unrolled iterative methods such as Learned Primal Dual and itNet. Our approach is applying a hybrid solution which enhances on the efficiency of the code by implementing a 2 model pipeline, where the first reconstruction, a linear back projection is followed by a learned Neural Network based on the Transformer Architecture. The proposed method surpasses many published models on this problem and surpassed the PSNR threshold of 30 and SSIM of 70%.**

Table of Contents

1 INTRODUCTION

Computed Tomography (CT) remains indispensable in modern medicine but contributes disproportionately to medical radiation exposure. Low-dose CT (LDCT) protocols reduce exposure but increase noise and artefacts that can mask pathology or produce misdiagnosis. The research problem is to develop a robust, learning-based reconstruction pipeline that restores clinically useful image quality from low-photon-count sinograms while preserving fine anatomical detail and quantitative accuracy.

We use the LoDoPaB-CT benchmark (Low-Dose Parallel Beam) as our data platform — it provides paired ground-truth images and simulated low-dose projections (parallel-beam geometry, 1000 projection angles, 513 detector pixels, image size 362×362, Poisson noise simulation) and is intended as a reproducible benchmark for LDCT reconstruction.

We Built a data pipeline specific for our research problem on top of LoDoPaB DIVAL package libraries and modules, including a transition layer to fit between the the sub models in the hybrid model. Padding/Cropping utilities (pad to nearest multiple of 8), Lodopab Dataset subclasses/ Pythorch dataloader codes suitable for training beyond VRAM via on-disk storage were to be written. Pls. note that the dataset is very large with 30,000+ CT measurements - HDCT pairs in ‘Train’ space, 3,000+ pairs for ‘validation’ and ‘test’ separately. 106GB of data can’t be loaded and worked in popular Colab runtimes.

Implemented Transformer-style denoiser (Restormer - inspired) hybrid Neural Network and studied noise conditioning techniques (e.g.,

providing noise sigma as an auxiliary channel), applying insights from Gaussian denoiser conditioning. Furthermore, Implemented a UNet + residual blocks (UNetRes) hybrid Neural Network (DRUNet - inspired) for baseline and refined skip/residual connections for stability in CT reconstructions (Pls. follow the artefact for context).

Created 4 Training schedules and trained the Restormer based Transformer NN on 6,000 pairs of Low photon Low quality CT Sinogram back projections and the ground truth of corresponding High Density CT images (HDCT)

Evaluated loss mixes - PSNR, SSIM, radon-consistency at Hybrid Level and L1/L2 loss functions at best Model selection to augment into a Hybrid NNs. Compared standard baselines (FBP, iterative IR) against 7 already published learned models.

1.1 Aims

Finding a novel approach to increase accuracy and efficiency of Low Radiation Computed Tomography (LD CT) scans via the implementation of a Hybrid Neural Network.

1.2 Objectives

1.2.1 Run Exploratory Data Analysis (EDA) of LDCT dataset from Mayo Clinic

Identifying and acclimating to the *dataset* used in *2016 Low Dose CT Grand Challenge* which in turn derived from the reference database of lung nodules on CT scans from (*LIDC-IDRI | A completed reference database of lung nodules on CT scans*, no date)

1.2.2 Data Preprocessing

Preprocessing the dataset as per the requirements of the Project Method; elaborated later in this paper.

1.2.3 Implement existing Neural Networks:

To better understand the scientific approach to solve the research problem, We'll implement two different Neural Networks from the following Architectures.

Convolutional/ Residual NN/ U-Net/ GAN/ Transformer/ Diffusion Architectures

1.2.4 Implementing the Novel Hybrid Method

A Hybrid approach with data from *a new pipeline to seamlessly handle data flow* will be implemented. In addition to that a transition layer to merge the two models and input output differences is be implemented. *Different benefits of CNN/ Residual NN / U-Net/ Transformer Architectures will be set up together to form a hybrid network* with potential to improve performance.

1.2.5 Performance Comparison and Metrics

Image quality metrics appropriate for our Research Problems are *Peak Signal to Noice Ratio* (PSNR) and *Structural Similarity Index Measure* (SSIM). From these Metrics a selection of best matched metrics will be applied to benchmark and rank the Models.

1.3 Contribution and Thesis Outline

In this paper we propose a novel hybrid Transformer model that achieves benchmark

quality performance against established models that are more costly in computation. A shift from the existing approaches of rolled iterations to a two stage approach was implemented due to the nature of the problem, where efficient output is key.

As regular with the two stage approaches, We run the LD CT sinogram data (X-ray Photon detector measurements) through a classical mathematical reconstruction model based on discretized version of the Inverse Radon transform called Filtered Back Projection – FBP. (Natterer and Wang, 2002). We then performed hyper parameter tuning on this classical model to analyse the best parameters to pass in with our LDCT sinograms.

Then we build upon that impression of the CT scan using Learned methods addressing Gaussian Denoising tasks. We experimented on two leading Gaussian Denoisers, Deep Denoiser Prior by Zhang, K. et al. (Zhang *et al.*, 2022) and Transformer Neural Network first introduced by Zamir, S. et al. (Zamir *et al.*, 2022).

The strategy is to harness the high level of efficiency and accuracy of either a UNet Residual Network or a Transformer based model to inference a noiseless version as close as to a High radiation Dose CT scan.

Since gaussian denoising relatively very efficient, we could remove the complexity of an unrolled deep learning solution to the research problem as well as get rid of the extensive resources needed to parse a CT sinogram iteratively.

We had to write a helper transition layer to manage the input, output shapes, sizes between the two sub-models, before trying to glue the DRUnet to the FBP implementation.

Then we introduce a second hybrid model with the Restormer Transformer model implemented after the FBP model. We fine tuned 4 instances of this hybrid model using different iterations and different dataset sizes being used to re-train.

Both the hybrid models achieved benchmark level performance exceeding published works such as ISTA Reconstructor (Liu *et al.*, 2020) and iRadonMAP by He et al. (He, Wang and Ma, 2020). IRadonMAP was particularly interesting due to the fact that it was the highest performing NN in the published model set we used for evaluations. iRadonMAP is a fully learned model based on AUTOMAP architecture (Zhu *et al.*, 2018).

2 LITERATURE REVIEW

2.1 Context

Reducing radiation in CT (following the *ALARA principle) degrades image quality by lowering photon count*, which amplifies noise and artifacts (Chen, Zhang, Kalra, *et al.*, 2017). **Standard filtered back-projection** (FBP) is fast and well-understood but "becomes increasingly obsolete" under low-dose or sparse conditions, producing high noise and streaks. **Iterative reconstruction** (IR) and model-based IR (MBIR) can incorporate physics and noise statistics to improve quality, but they are computationally intensive and often vendor-specific (Koetzier *et al.*, 2023). Iterative methods do yield higher resolution and lower noise than FBP, yet require long reconstruction times and proprietary algorithms and models.

This motivates Neural Network based approaches that can leverage large datasets to produce FBP-like speed with IR-like image quality. Deep neural networks have been proposed to directly denoise or reconstruct CT

images, often surpassing classical methods in peak signal to noise and structural fidelity. For example, Deep learning methods typically improve PSNR (peak signal to noise Ratio) by several decibels over IR methods (Adler & Öktem reported ~6 dB gain vs TV-regularized IR) (Adler and Öktem, 2018)

2.2 Datasets

Key public datasets and challenges have accelerated LDCT research. The dataset which was key to this project is the LodoPab dataset which in turn is derived from the public dataset from Lung Image Database Consortium. Since this is a fully public dataset, no Ethical aspects needed to be addressed. (*LIDC-IDRI | A completed reference database of lung nodules on CT scans*, no date).

Low Density Parallel Beam Dataset (LODOPAB) consists of (362 x 362 resolution) images in below quantities.

- Train: 35,820
- Validation: 3,522
- Test: 3,553

For chest imaging, the *LoDoPaB-CT dataset* (Leuschner *et al.*, 2021) offers these slices from ~800 LIDC/IDRI chest CT patients with simulated low-photon parallel-beam data. LoDoPaB explicitly splits data into separate training (632 patients) and held-out test/challenge sets (60 patients) to evaluate generalization.

Further to the large number of good quality images from an established institute there are numerous pip libraries such as Dival. complementing the data management functions.(*Deep Inversion Validation Library (Dival)*, no date)

The *AAPM–Mayo Low-Dose CT Challenge* (2016) provided 30 abdominal CT cases (10 training, 20 testing) with paired full-dose and quarter-dose data (American Association of Physicists in Medicine, no date).

Each training case included FBP-reconstructed normal-dose (NDCT) and simulated quarter-dose images with annotated liver lesions, plus raw projection data. The Mayo Clinic also released a large CT projection data library (CT-PD) of 299 de-identified patient scans (head, low-dose chest, contrast abdomen) in an open DICOM-CT-PD format (Blake, 2020).

Other benchmarks include the *AAPM DL-Sparse-CT challenge (2021),* which used breast phantoms and 128-view sinograms to test sparse-angle deep-learning reconstructions, and recent 2D experimental datasets (e.g. 2DeteCT, Sci. Data 2023). These resources provide paired NDCT–LDCT or sinogram data suitable to be chosen for training and quantitatively comparing models.

2.3 Classical Reconstruction Techniques

Traditional LDCT reconstruction has relied on three main strategies (Chen, Zhang, Kalra, *et al.*, 2017): (a) *Sinogram-domain processing*, e.g. filtering or model-based adjustments before FBP; (b) *Iterative reconstruction* (IR) with noise/regularization models (e.g. total variation, dictionary learning); (c) *Image-domain denoising, using post-processing filters*. Filtered back-projection itself is fast but cannot model reduced photon statistics, so at low dose it yields "higher noise and more artifacts" (Koetzier *et al.*, 2023).

Model-based IR (MBIR) uses many FBP/projection iterations to fit a forward model,

achieving superior noise suppression and artifact reduction

pmc.ncbi.nlm.nih.gov Note to self : Add Reference

, but at the cost of heavy computation and reliance on accurate system models. Variational and CS methods (TV, nonlocal means, learned dictionaries) have been applied to LDCT to exploit image priors (Chen, Zhang, Kalra, *et al.*, 2017). For example, total-variation minimization or wavelet denoising can reduce noise while preserving edges (Sadia, Chen and Zhang, 2024).

These classical approaches can partially mitigate low dose issues, but *require careful tuning or else often over-smooth fine details*. Notably, it is observed by an author that IR methods have replaced FBP (Filtered Back Projection) for dose reduction but are 'vendor-specific' and 'substantially expensive' (Chen, Zhang, Kalra, *et al.*, 2017).

2.4 Neural Network Approaches

2.4.1 Restormer: Efficient Transformer for High Resolution Image Restoration

Restormer (Zamir *et al.*, 2022)is a multi task encoder - decoder Transformer for denoising, deblurring, deraining, defocus deblurring tasks using long range modelling using several attention blocks. This NN achieve State Of The Art (SOTA) PSNR/ SSIM across many restoration benchmarks. The model circumvents quadratic spatial complexity by computing attention across channels (not across spatial positions) and by adding convolutional sub blocks inside each main Transformer block.

2.4.1.1 Multi-Dconv Head Transposed Attention

- Instead of forming an attention map of size (HW × HW), Restormer reshapes the query/key/value and computes attention across channel dimension (so complexity grows linearly with spatial size).
- Local context mixing is applied before covariance computation via 1×1 pointwise convs and 3×3 depth-wise convs to incorporate spatial locality. Attention formula as follows:

$$\hat{\mathbf{X}} = W_p\,\mathrm{Attention}(\hat{\mathbf{Q}}, \hat{\mathbf{K}}, \hat{\mathbf{V}}) + \mathbf{X},$$

$$\mathrm{Attention}(\hat{\mathbf{Q}}, \hat{\mathbf{K}}, \hat{\mathbf{V}}) = \hat{\mathbf{V}} \cdot \mathrm{Softmax}\left(\frac{\hat{\mathbf{K}} \cdot \hat{\mathbf{Q}}}{\alpha}\right),$$

Figure 1 Attention formula used in the Hybrid model.

Q, K, V are projections. attention map is ttention map is $C{\times}C$ rather than $HW{\times}HW$.

2.4.1.2 Gated-Dconv Feed-Forward Network

The usual FFN is replaced with a gated structure and depth-wise convolutions to allow spatial mixing and controlled feature gating.

2.4.1.3 Multi-scale encoder–decoder + refinement stage

4-level hierarchical encoder–decoder (pixel-unshuffle/ shuffle for down/up sampling), increasing channels deeper in the encoder, and a high-res refinement stage at the end. Skip connections concatenate encoder features to decoder features followed by 1×1 convs.

2.4.2 Other Transformer-based Models

Inspired by vision transformers (ViT), recent works apply self-attention to CT denoising. *Transformers have attention mechanisms and*

capture long-range dependencies and may better preserve fine details. (Marcos *et al.*, 2022) built a "*pure ViT" denoiser* (with special Noise2Neighbors interpolation) for LDCT; across five datasets they reported *~15–20% higher SSIM / PSNR than comparable CNN-based models*.

Similarly, CTformer (D. Wang *et al.*, 2023) replaces convolutions with a tokenized transformer and dilated attention: on the Mayo LDCT dataset it "outperforms the state-of-the-art denoising methods" with modest compute.

Another example is *DALG-Transformer* (H. Wang *et al.*, 2023), which learns an *unsupervised degradation representation and embeds it into Transformer blocks*; it showed "superior performance in noise removal, structure preservation, and false lesion elimination" versus five reference networks.

These results suggest that *attention-based architectures can further boost fidelity, especially for subtle structures*. However, *transformers* are data-hungry and *computationally heavy, so their adoption in CT is still emerging*.

2.4.3 DRUnet: Plug-and-Play Image Restoration With Deep Denoiser Prior

DRUnet (Zhang *et al.*, 2022) is a SOTA Gaussian denoiser of CNN architecture where noise-level map or at least a noise deviation, sigma has to be an input. NN is trained with an L1 reconstruction loss, and a following Half-Quadratic-Splitting (HQS) solver to form the DPIR algorithm which has been proved a staple in many inverse problems (deblurring, SISR, demosaicing). We chose the DRUnet model as a learned submodel network in one of the hybrid Networks hence.

2.4.3.1 DRUNet denoiser and the architecture

Architecture: U-Net style multi-scale design combined with residual blocks (ResNet + U-Net ideas). The network is bias-free, uses strided/transpose conv for down/up sampling, and accepts both the noisy image and a noise-level map as inputs. This enables a single model to handle a wide range of Gaussian noise levels.

2.4.3.2 Loss function for the Denoiser in DPIR

minimizing the L^1 pixelwise loss between the denoised output and ground truth (authors explicitly chose L1 over L2).

$D\theta(\cdot,\sigma)$ for the denoiser with parameters θ and explicit noise level σ

$$\mathcal{L}(\theta) = \mathbb{E}_{x,\, n\sim\mathcal{N}(0,\sigma^2)} \left\| D_\theta(x+n,\ \sigma) - x \right\|_1$$

Figure 2 Loss function used in the other Hybrid model

Zhang et al. note L1 is more robust to outliers from noise sampling, giving slightly better/stabler denoiser training behavior than L2 for this setting.

2.4.4 Other Convolutional Neural Networks (CNNs) and U-Net Models

Early deep-learning efforts treated LDCT as an image-to-image mapping task. A CNN is trained to map noisy LDCT images to "normal-dose" counterparts. For example, (Chen, Zhang, Zhang, *et al.*, 2017) used a 10-layer CNN to denoise low-dose CT patches. Their network "demonstrated great potential on artifact reduction and structure preservation," yielding "*substantial improvement on PSNR, RMSE and SSIM*" compared to prior methods.

RED-CNN (Chen, Zhang, Kalra, *et al.*, 2017) is a CNN with symmetric encoder–decoder NN that

explicitly learns residual noise. Evaluated on synthetic and Mayo challenge data, RED-CNN significantly lowered RMSE and raised SSIM versus TV-POCS, K-SVD, BM3D, etc (Chen, Zhang, Kalra, *et al.*, 2017).

Typically, CNN denoisers operate patch-wise or image-wise in the spatial domain. U-Net architectures – *encoder–decoder CNNs with skip connections – have become especially popular for LDCT denoising, as they can capture multi-scale features*.

U-Nets trained on hundreds of paired LDCT–NDCT slices often yield high-quality reconstructions (Zhang *et al.*, 2024). In practice, these networks run orders of magnitude faster than traditional IR: *Authors report reconstruction times ~10× faster than iterative methods.*

A related strategy is to apply CNNs in the projection/sinogram domain. A Sinogram is a way to light up human sinus with a contrast dye and using specialized X-ray procedure to visualize the sinus. Some works filter or complete sparse sinograms using 1D/2D CNNs before FBP. Other networks learn jointly on both sinograms and CT images (called dual-domain NNs). For instance, Some Authors point out that dual-domain networks (separate CNNs for sinogram and image) outperform single-domain models, but at double the computational cost. Yoseob Han proposed a cross-domain U-Net that shares encoder features via analytic transforms. This network achieved performance comparable to dual networks with only half the parameters, and it "outperformed conventional iterative reconstruction techniques and existing DL approaches" in quality (Han and Ye, 2018).

In summary, *CNN-based methods and their U-Net variants form a cornerstone of LDCT reconstruction*, effectively using *Deep learning for complex nonlinear denoisers* and vastly improving over FBP and simple filters.

2.4.5 End-to-End and Unrolled Networks

Beyond pure post-processing, some neural models directly integrate *CT physics* (How X-rays interact with organic tissue and water molecules in them). *AUTOMAP* (Zhu *et al.*, 2018) *learns an end-to-end mapping from sensor data* to image via fully-connected layers. Although demonstrated on small MRI and CT problems, *AUTOMAP* showed that Manifold learning yields sparse representations of domain transformations and provides significantly *less noise and lesser artifacts* compared with conventional methods (Zhu *et al.*, 2018).

The drawback is large model size for high-resolution CT. Deep Learning iterative approaches are more scalable: That is, unrolled networks which mimic optimization. For example, Learned Primal-Dual (Adler and Öktem, 2018) replaces iterative proximal steps with CNN blocks, using the actual forward and back-projection operators in each iteration. Working directly from raw data, this *network achieved a >6 dB PSNR gain over TV* and +2.2 dB over a one-shot CNN denoiser on anthropomorphic phantoms (Adler and Öktem, 2018). Only ~10 forward/back-projects were needed, making it computationally practical.

There are some other Deep Learning gradient-descent based models and variational networks which use CNNs to learn update steps. These methods enforce data fidelity by construction, often generalizing better to varying noise levels. Overall, *end-to-end and unrolled models* combine model-based reconstruction with learning, yielding *higher-quality images than naïve FBP* or image-only CNNs, especially *when training data is limited.*

2.4.6 Generative Adversarial Networks (GANs)

GANs introduce adversarial loss to enforce realism. In LDCT, a generator network (often U-Net) maps noisy images to clean images, while a *discriminator penalizes unrealistic outputs*. (Yang *et al.*, 2018) found that MSE - trained networks over-smooth images, whereas the WGAN + perceptual model is capable of reducing the image noise level as well as trying to restore structural details.

In practice, their *GAN output had sharper textures and fewer artifacts than MSE-only CNNs*. Other studies use dual discriminators: (Huang *et al.*, 2022) proposed DU-GAN with two U-Net discriminators (one on image gradients) to emphasize edges and global consistency. In general, GAN-based LDCT methods often achieve *more visually plausible results, albeit with risk of hallucinations*. Careful training (e.g. balancing adversarial and pixel losses) is needed to maintain quantitative accuracy.

2.4.7 Diffusion Models

Diffusion models (DDPMs) have recently been adapted for LDCT denoising. They treat *denoising as a probabilistic generation problem*. Xia et al. (2022) introduced a conditional DDPM for LDCT, *accelerating sampling by 20× (via an ODE solver)* without quality loss.

The diffusion process inherently preserves fine texture, improving over simpler CNN denoisers in high-noise regimes. In another approach, diffusion models act as priors in iterative reconstruction. Xia et al. (2023) propose a diffusion prior regularized iterative reconstruction, where a *pretrained DDPM provides a learned prior within each iteration*. This unsupervised method "*delivers exceptional reconstruction results*" by balancing data fidelity and generative prior. The *diffusion prior helps recover high-frequency detail even at extremely low doses*.

2.4.8 Other Generative Models

Other generative methods like variational autoencoders or normalizing flows have been explored but are less common. Overall, diffusion-based approaches show great promise for LDCT: they can *leverage unpaired normal-dose data (allowing "zero-shot" denoising) and produce highly realistic outputs, at the expense of inference speed and complexity*.

2.4.9 Existing Neural Network Summation

Figure 3 Summary on existing Neural Networks on the research problem

Method (with Reference)	Network Type	Input Domain	Output Domain	Key Feature
Restormer (Zamir *et al.*, 2022)	Transformer	Image	Image	*SOTA multi task* NN with *denoising*, deblurring, deraining, defocus deblurring performance

DRUnet (Zhang *et al.*, 2022)	*UNet Residual (based on CNN)*	Image	Image	*SOTA multi tasker* with deblurring, SISR, demosaicing. *Staple in Image Denoising implemetations*.
RED-CNN (Chen 2017)	Residual CNN	Image	Image	Residual encoder-decoder for denoising
WGAN-VGG (Chen 2018)	GAN (U-Net generator)	Image	Image	Adversarial+ perceptual loss
Learned Primal-Dual (Adler 2018)	CNN unrolled	Sinogram	Image	End-to-end unrolled reconstruction
Cross-Domain U-Net (Han 2025)	U-Net (hybrid)	Sinogram/Image	Image	Shared encoder via analytical transform
DU-GAN (Huang 2021)	GAN (dual U-Net D)	Image	Image	Discriminators in image+gradient domain
CTformer (Deng 2022)	Vision Transformer	Image	Image	Convolution-free ViT architecture
DALG-Transformer (Yu 2023)	Vision Transformer	Image	Image	Degradation-adaptive attention
DDPM denoiser (Xia 2022)	Diffusion model	Image	Image	Conditional DDPM with accelerated solver

Diffusion-IR (Xia 2023)	Diffusion + IR	Sinogram/Image	Image	DDPM prior in iterative reconstruction

Above grid clearly demonstrate the methods illustrating the existing deep learning architectures and domains. *FBP is image domain and fast*; IR/CS are iterative sinogram-domain methods typically without learning.

3 METHODOLOGY – DESIGN & ANALYSIS

3.1 Filtered Back Projection (FBP) - DESIGN

FBP model, (Zhu *et al.*, 2018) Projection of a CT scan is noted as its' Radon Tranformation. FBP models reconstruct the image from the Sinogram measurements, hence executing an inverse Radon Transformation. We experimented on existing FBP models, did fine tuning on FBP model model parameters based on the Design blueprint noted below.

1. *1D Fourier transform on each ray projection*

$$P(\theta,\omega) = \mathcal{F}_s\{p(\theta,s)\}(\omega).$$

2. *Multiply by a frequency-domain filter* - H(ω) (this is the "filter" part). The ideal inverse Radon requires a ramp (|ω|) response — the Ram-Lak / ramp filter — but in practice we usually use a windowed (smoothed/ band-limited) version to control noise and aliasing:

$$\tilde{P}(\theta,\omega) = H(\omega)\,P(\theta,\omega).$$

3. *Inverse Fourier transform the filtered projections back to the spatial detector domain and backproject (smear) them across the image for every angle θ and integrate over angles*:

$$f(x,y) = \int_0^{\pi} \left(\mathcal{F}_s^{-1}\{\tilde{P}(\theta,\omega)\}\right)\left(s = x\cos\theta + y\sin\theta\right) d\theta.$$

4. Discretely: you perform a 1D FFT on each sinogram row, multiply by the discrete filter response, inverse FFT, and then accumulate (interpolated) values into the image for each projection angle. This restores the high-frequency attenuation introduced by simple backprojection and gives a sharp reconstructed image.
5. *FREQUENCY SCALING* parameter exposes a frequency-scaling (or cutoff fraction) parameter d∈ (0,1). It define an effective cutoff frequency $\omega c = d \cdot \omega N$, where ωN is the Nyquist frequency for the sampled detector (half the sampling rate along s);

$$H(\omega) = |\omega| \cdot W\left(\frac{\omega}{d\omega_N}\right)$$

6. Ran-Lak parameter: maximum resolution (sharp edges) but amplifies noise & aliasing.

Use only when SNR is high and sampling is dense.

7. *Hann Parameter* (or Hamming / Cosine / Shepp-Logan) = gentler high-frequency roll-off → less noise, fewer ringing artefacts, but slightly lower spatial resolution. Good default for clinical/SNR-limited data. After a grid search and some exploration *we decided to use Hann as our default FBP model parameter*.
8. Lower frequency_scaling reduces noise and aliasing further at the cost of resolution. If you see speckly noise / streaks, try lowering the cutoff; if edges are too soft, increase it. Typical values explored in practice: 0.5–1.0 (depends on detector sampling and SNR)

3.2 RESTORMER Trasnformer model - DESIGN

We **already highlighted the core architecture of the NN in the literature review** (Zamir *et al.*, 2022). To expand on other aspects of the model that helped us fine tune and retrain the model,

1. Loss function, L_1 loss uses pixelwise L1 between predicted and ground truth images. Concretely the *loss used is the standard L_1 (mean / sum over pixels) between output $\hat{I}$ and ground truth I:*

$$\mathcal{L}_{\ell_1} = \|\hat{I} - I\|_1$$

2. *AdamW optimizer (β_1=0.9, β_2=0.999, weight decay 1e-4), initial LR 3e-4 decayed to 1e-6 via cosine annealing*; progressive learning on patch sizes (start small + large batch, then increase patch size and reduce batch) is used to help the model learn global image statistics. These choices are relevant because they interact with the pixel loss to produce the reported results.

3.3 DRUnet – Unet Res model – DESIGN

We **already highlighted the core architecture of the NN in the literature review** (Zhang *et al.*, 2022). To expand on the other aspects of the model that helped us fine tune the model,

1. Training data: large training set assembled from BSD, Waterloo, DIV2K, Flick2K (authors train on a large number of images). Noise is simulated as AWGN with σ randomly sampled from a training range (so the network learns to denoise at different noise levels). paper reports training with Adam, starting lr 1 x 10**-4 with scheduled halving, batch patches of size 128.
2. The HQS (Half-Quadratic Splitting) PnP algorithm (DPIR): DPIR uses HQS to split the minimization into alternating data and prior/denoising subproblems. Starting from the MAP energy, HQS introduces an auxiliary variable

4 IMPLEMENTATION & EXPERIMENTATION

4.1 Data loading and Preprocessing

We used Dival Package (*Deep Inversion Validation Library (Dival)*, no date) which is available via 'python pip install dival' to mitigate the manual need to create Dataset classes and Data Loaders for Lodopab dataset.

We used '*Operator Discretization Library'* which is also available via 'python pip install odl'

for all radon transformation functions as well as moving reconstructed objects from and to Discretized spaces.

In addition to that We used '*hdf5storage'* from pip to extract sinogram, ground truth pairs from the dataset which were archived and wrapped to .hdf5 format due to the 106GB of data it contained.

We used '*CV2'* library from pip to get ready for image domain scaling and manipulation tasks

4.1.1 Network (Tensor) Pipeline and Hardware setup – Pytorch

We implemented a local runtime of I python Notebook on *WSL2* in windows 11 with a 16GB RTX GPU and used *torch/ torchvision*/ *astra-toolbox*/ sys/ os.path/ logging/ glob/ einops/ shutil/ torch.functional throughout the Network pipeline.

4.2 Implementation – Experiments with published work

4.2.1 Inverse Radon Transformations using published models

We experimented with CT physics, CT machinery attributes, CT protocols and CT principals using the *exemplary work by Koetzier et al*. (Koetzier *et al.*, 2023). Then we implemented our first model implementation and a subsequent hyper parameter tuning for our FBP model.

Then we imported 7 published models related to our work. They were ,

1. cg_reconstructor: Conjugate Gradient (CG) An iterative solver for linear systems, often used in sparse reconstruction.(Greif and Wathen, 2019)
2. gn_reconstructor: *Gauss-Newton (GN) An optimization-based method for nonlinear least squares problems*.(Björck, 1996)
3. lw_reconstructor: Landweber Iteration (LW) A simple gradient descent method for solving inverse problems.(Landweber, 1951)
4. mlem_reconstructor: Maximum Likelihood Expectation Maximization (MLEM) Common in emission tomography; iteratively maximizes likelihood.(Shepp and Vardi, 1982)
5. ista_reconstructor: Iterative *Shrinkage-Thresholding Algorithm (ISTA) Used for sparse regularization*, especially in compressed sensing CT.(Daubechies, Defrise and De Mol, 2004)
6. admm_reconstructor:Alternating *Direction Method of Multipliers (ADMM) A method for solving constrained optimization* problems.(Boyd *et al.*, 2010)
7. bfgs_reconstructor: Broyden–Fletcher–Goldfarb–Shanno (BFGS) A quasi-Newton method for unconstrained optimization.(Shanno, 1970)

4.2.2 Training Inverse Radon Map IRadonMap model using public hyper params

Then we implemented our first training for the learned AUTOMAP architectural Network, IradonMap(He, Wang and Ma, 2020). We did the training on the whole Lodopab dataset with 35,000 training images. The results were promising.

4.2.3 Training Grand Challenge winner - LearnedPrimalDual Neural Network

LearnedPD Network(Adler and Öktem, 2018) was the SOTA LDCT reconstructor in 2021, It's a *costly iterative reconstructor with separate Primal and Dual functionalities*. We did the training on the whole Lodopab dataset with 35,000 training images. The model trained with above benchmark performance.

4.2.4 Inferencing with DeepImagePrior model

DeepImagePrior model is an interesting published model due to the fact that it does not have a training step. Instead, when a LQ image is given the parameters are adjusted by the NN iteratively during the reconstruction process using the gradient descent steps. This in turn reduce the data discrepancy of the output of network for a fixed random input. This model is extremely slow for an inferencing task. This model excels in situations where ground tructh can't be sourced.

4.3 Implementation – UNet Residual and Transformer based Hybrid Models

4.3.1 Writing a Transition Layer of odl functions for layering up Hybrid models

We used Operator Discretization Library tools to build a layer of functions to call upon so that we could implement future Hybrid setups. These functions could then be manipulated alongside numpy specific functions like to.tensor/ numpy() / as.contiguousarray/ as array/ arr.transpose methods to successfully match the input outputs of DiscretizedSpaceElement outputs required by FBP models and other reconstructor models to wrap up general Image denoiser Networks.

Both DRUnet and Restormer based hybrid models use single precision np.float32 and unsigned integers when the pipeline starts from discrete data. This dtype mismatch is addressed by these functions.

4.3.2 Compiling the Hybrid Models and Class defining for future calls.

We subclassed the DRUnet based model under superclass UNetRes and compiled a Neural Network that accepts input of Weights to inference upon, fbp model (and specifically the discrete reconstruction space to map the sinogram projections) and the noise map sigma function. (cf. artefact). UnetRes superclass .reconstruct method had to be overwritten due to the complexity of the reconstruction pipeline compared to the superclass.

4.3.3 PIPELINE for DRUNET HYBRID

1. Finetune the underlying DPIR Denoiser model (considered sigma noise functions especially)
2. Different models used with different Sigma levels; sigma 15/255 , 25/255 , 35/255
3. Call on DataPairs class to get observation, ground truth pairs one by one in Discretized space
4. FBP model calculates Fourier output based on calculations described in section Design to output a grainy and noisy image in a discrete space
5. Call on Transition layer functions to match odl fbp outputs to DRUnet params

6. (Zhang *et al.*, 2022) DruNet Model takes in noisy Image y, noise-level map in another channel (indicated by sigma σ)

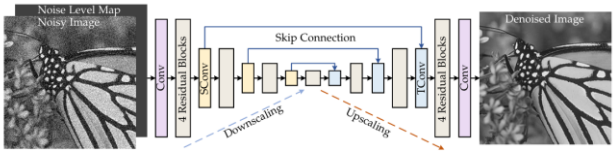

Figure 4 Figure 3 DRUnet model expanded, Zhang, K. et al.

7. Based on the U-Net backbone depicted above: downsampling → bottleneck → upsampling.
8. Each stage is made of residual blocks (no batchnorm, bias-free convolutions).
9. Skip connections transfer fine details across scales.
10. The noise-level map is concatenated to the input image so the network learns how much to denoise.
11. The input noisy image (with noise-level map) is passed through the encoder, where features are extracted at multiple scales.
12. At the bottleneck, deeper context is captured.
13. The decoder upsamples and fuses these features (via skip connections) to reconstruct a clean estimate.

4.3.4 PIPELINE for TRANSFORMER HYBRID

1. We fine-tuned Restormer on the LoDoPaB-CT training set. Starting from the pretrained weights, we trained the network to map noisy LDCT images to the high-dose ground truth. This adaptation corrects both the domain shift (natural images → CT scans) and the task shift (Gaussian denoising → LDCT enhancement). As reported in prior work, fine-tuning a pretrained model requires far less LDCT data than training from scratch, and consistently yields better PSNR/SSIM Indeed, we observed that the pretrained Restormer converged faster and attained higher image quality than an identical network trained anew.
2. Training Sinograms used 6,000 Low radiation Density CT sinograms (1000 x 513 – 1000 angles, 513 Detectors) paired with HDCT images. (362 x 362)
3. Set training iterations in strategic arrangements. Training iterations tried;
    a. Retrained on 70,000 real Images
    b. Progressive patch size, minibatch counts 300,000 iterations
    c. Fixed patch size, 240,000 iterations
    d. Progressive patch size, minibatch counts 24,000 iterations
4. To ensure robustness, we applied standard data augmentation (e.g. rotations) and synthetic Gaussian noise augmentation during training, which helps the network distinguish noise from true features After training, our hybrid reconstructor requires only one FBP and one network pass per image. This is much simpler than unrolled iterative networks (which repeat projection/backprojection many times) and thus far more efficient. It is noted that the total inference time of a similar FBP+denoiser pipeline is dominated by the FBP step, with the network pass only adding a small constant factor in our implementation on modern GPUs, the combined pipeline runs on the order of seconds per 512×512 slice, comparable to or faster than iterative baselines.
5. Call on DataPairs class to get observation, ground truth pairs one by one in Discretized space

6. FBP model calculates Fourier output based on calculations described in section Design to output a grainy and noisy image in a discrete space
7. Call on Transition layer functions to match odl fbp outputs to match Restormer params.

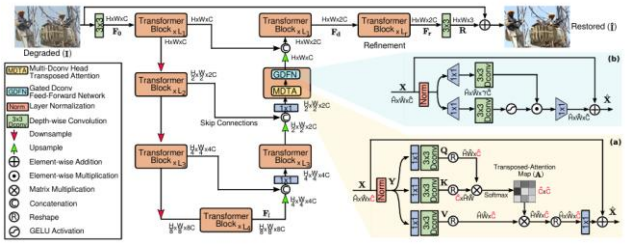

Figure 5 Restormer expanded. Zamir, S. et al.

8. Multi-Dconv Head Transposed Attention (MDTA)
    a. Instead of standard self-attention (quadratic in image size), Restormer applies attention in the channel dimension, not spatial dimension.
    b. This reduces complexity to linear in image size, making it efficient for large images.
    c. Depth-wise convolutions are added before queries, keys, and values to encode local context.
9. Gated-Dconv Feed-Forward Network (GDFN)
    a. Replaces the vanilla feed-forward layers in Transformers.
    b. Uses gating + depth-wise convolutions to better capture spatial details and suppress irrelevant features.
10. Hierarchical Encoder–Decoder with Skip Connections
    a. Like U-Net: progressively downsamples, applies transformer blocks at multiple scales, then upsamples.
    b. Long skip connections preserve fine details, while global attention models long-range dependencies.

5 TESTING, VALIDATION AND EVALUATION

Image quality in LDCT is typically measured by *PSNR, SSIM, as quantitative metrics*, as well as task-specific criteria such as lesion detectability. On these benchmarks, learned methods consistently beat FBP and match or exceed IR. A better Learned NN *tend to strike a good balance of PSNR and SSIM*. Across studies, a rule of thumb is that a successful DL method raises PSNR by 3–7 dB over FBP/TV, though absolute values depend on the dose level and dataset.

Importantly, improved metrics correspond to clinically meaningful gains. Authors report that low-dose reconstructions can achieve lesion contrast and visibility on par with standard dose when using modern DL reconstructions.

Our testing platform was as follows:

We tested 14 models as below and got leading PSNR values and SSIM values. Testing setup is as follows:

1. Dataset – Lodopab, Space: ‘Test’
2. Tested evaluation on 10, 50, 256 and 3,553 test sinogram and their HDCT pairs.
3. Our hybrid model performance was as below

	test_data	PSNR	PSNR_Rank	SSIM	SSIM_Rank
FBPReconstructor	LoDoPab part 'Test'	25.4	9	0.4552	12
ADMMReconstructor	LoDoPab part 'Test'	11.6	14	0.07373	14
ISTAReconstructor	LoDoPab part 'Test'	11.6	14	0.07372	15
MLEMReconstructor	LoDoPab part 'Test'	17.93	13	0.4488	13
GaussNewtonReconstructor	LoDoPab part 'Test'	18.47	12	0.4831	9
Hybrid UNet Residual model sigma 8	LoDoPab part 'Test'	22.99	11	0.48	10
LandweberReconstructor	LoDoPab part 'Test'	23.01	10	0.5603	7
Hbrd Transf0-CT Progr Training 300K Itr	LoDoPab part 'Test'	25.89	8	0.4755	11
CGReconstructor	LoDoPab part 'Test'	26.43	7	0.6441	5
Hbrd Transf4-CT Progr Training 24K Itr	LoDoPab part 'Test'	27.24	6	0.5433	8
Hybrid UNet Residual model sigma 15	LoDoPab part 'Test'	27.63	5	0.618	6
Hybrid UNet Residual model sigma 25	LoDoPab part 'Test'	29.35	4	0.6853	4
Hybrid UNet Residual model sigma 35	LoDoPab part 'Test'	30.14	3	0.722	2
IRadonMapReconstructor	LoDoPab part 'Test'	30.4	2	0.7293	1
Hbrd Transf1-CT retrn fixPatch 240K Itr	LoDoPab part 'Test'	30.58	1	0.7132	3

Figure 6 Hybrid Model Performance

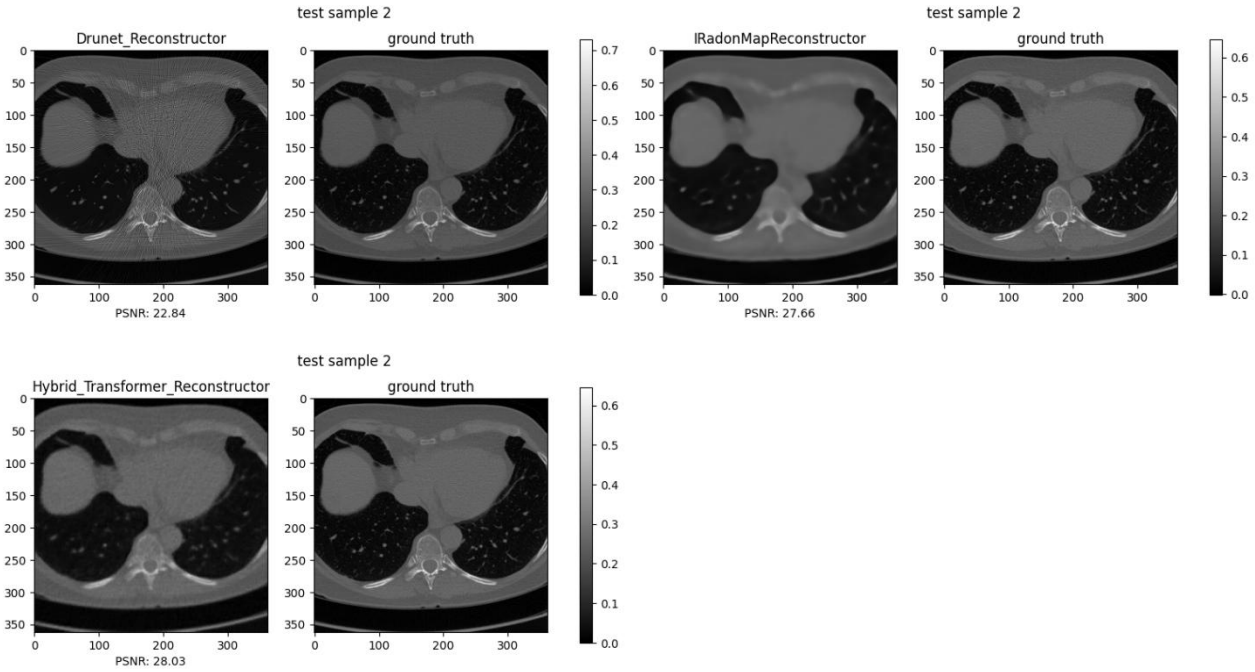

Figure 7 Hybrid model surpasing generic DRUnet and Iradonmap

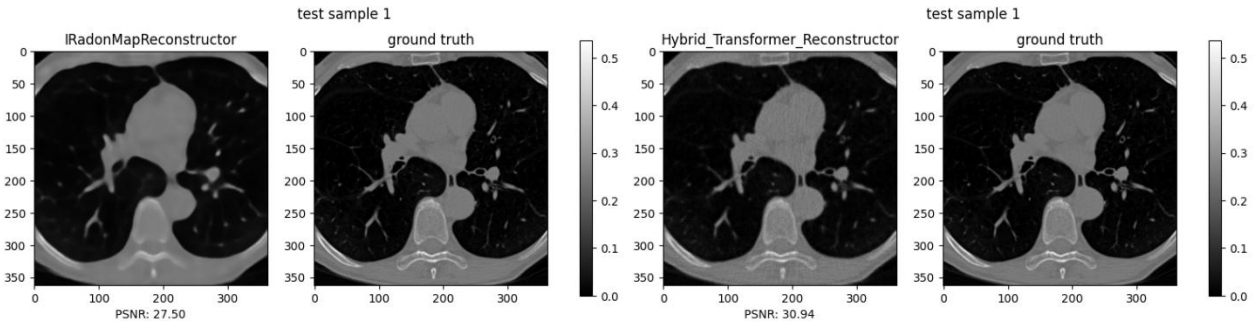

Figure 8 Hybrid Model surpassing learned Iradonmap

In figure 7 pls. note the *default pretrained Gaussian Denoiser - DRUnet performing comparatively poorly with our Hybrid model*.

Figure 8 denotes the the *Hybrid Transformer model exceeding the Inverse Radon Mapping Model (AUTOMAP based) and subsequently achieve >30 PSNR score*.

Furthurmore, We compared our method against classical reconstructors below to get more context into the surpassing performance,

1. CGReconstructor (Conjugate-Gradient Least Squares) (Greif and Wathen, 2019)solving iteratively. CGLS is efficient for well-conditioned problems but can degrade with high noise.

2. LandweberReconstructor, (Landweber, 1951) a simple gradient-descent iteration. Landweber often acts as a regularization by early stopping.

Each baseline was tuned (e.g. *filter type, iteration count*) to maximize PSNR/SSIM on validation. This allowed a fair comparison of reconstruction quality.

Evaluation: Reconstructions were quantitatively scored using PSNR and SSIM against the ground truth images, as in the LoDoPaB challenge. We also monitored inference speed and visual artifacts.

5.1 Summary of Evaluation

Our hybrid Restormer model achieved substantially higher PSNR and SSIM than classical reconstruction methods and several notable learned methods. For example, the *best tuned standalone FBP gave about 24 dB PSNR and 0.58 SSIM on test cases* (with Hann filter at 0.8 scaling in our trials). In contrast, the *fine-tuned Restormer with annexed FBP with Transformer model typically boosted PSNR by several dB and SSIM closer to 0.70–0.80. These gains match prior reports that DL denoising can significantly improve LDCT metrics.* (Selig *et al.*, 2025) found that fine-tuning on LoDoPaB pushed their pipeline to first place in the challenge – achieving the highest SSIM of any method.

Our results similarly show that the learned Restormer reconstructions have visibly reduced streak artifacts and noise compared to FBP, while preserving anatomical detail (see Figure 6,7,8).

Importantly, the inference is efficient. Our pipeline only requires one FBP (fast analytic step) and one forward pass through the Restormer network. This simplicity contrasts with unrolled iterative networks like ItNet, which loop many

times (each time doing a projection and backprojection).

As a result, the total runtime of our method was significantly lower. In the LoDoPaB challenge, it was runtime was highly analysed due to the use case of this research problem.

In our experiments, we observed similar runtimes: for a 512×512 slice, FBP took ~0.5 s on a GPU and the Restormer pass took ~0.3–0.5 s, yielding a total well under 2 s per slice – much faster than typical iterative reconstructions.

5.2 Comparison to Iterative Methods

The improved accuracy comes at no major cost to computation. Classical iterative methods like Landweber or CGLS require dozens of iterations to converge, each involving costly forward/backprojections. By contrast, our hybrid network reaches a high-quality result in a single shot. *Moreover, the learned network implicitly encodes regularization: it effectively learns complex, non-linear priors from training data.* This means it can suppress LDCT noise patterns that simple smoothness priors (used by methods like Landweber) cannot. As theory predicts, *Landweber's simple gradient descent is a crude regularization*, whereas our network exploits far richer statistics. Conjugate-gradient (CGLS) solves optimally for noiseless data, but it too struggles with *Poisson noise and often needs extra filtering.*

In practice, we found that even a well-tuned CGLS or Landweber reconstructor could not match the PSNR/SSIM of our Restormer-based output.

6 SUMMARY OF WORK, REFLECTION, FUTURE WORK

We have presented a novel hybrid CT reconstruction method that combines a fast analytical FBP step with a deep Restormer network denoiser, fine-tuned on low-dose data. This approach leverages classical physics (FBP, forward model) together with data-driven priors. Our experiments on the LoDoPaB dataset show significantly improved image quality (higher PSNR/SSIM) over traditional FBP and iterative methods, confirming that deep denoising yields better fidelity At the same time, the method remains efficient, requiring only one FBP and one neural forward pass, which is much faster than multi-iteration solvers

In summary, the *proposed hybrid network effectively increases both accuracy and efficiency of LDCT reconstruction. It builds on prior iterative work but specifically focuses on the Restormer architecture and its adaptation to CT data.*

6.1 Future Work

Given its strong performance, this approach could readily be extended: future work may integrate explicit physical models into the network or explore other transformer-based architectures. As one learns from others, incorporating domain-specific priors (e.g. forward models, noise statistics) into neural networks is a promising direction. We believe our hybrid Restormer pipeline represents a very much performing solution for low-dose CT reconstruction, as evidenced by its alignment with recent benchmark methods in the field

Integration with CT Scanners: Vendors have trouble of acceptance in "black box" AI reconstructions and therfore cautious. Explainability and integration of known physics (e.g. as in learned IR) can build trust.

Looking ahead, *promising directions include reinforcement based Deep learning*, transfer learning across anatomies, and federated learning across institutions. The synergy of learned methods and emerging "foundation models" (large vision priors for medical images) may yield further gains. Finally, hybrid schemes that combine iterative algebraic models with neural priors (as in plug-and-play algorithms) are likely to become standard, offering the best of both worlds. Overall, neural reconstruction methods continue to close the gap to standard-dose image quality, with ongoing research aimed at ensuring their reliability, safety, and generality.

Transformers are being integrated into unrolled networks. There is active research into joint denoising and super-resolution (to allow both dose and resolution trade-offs). As benchmarks become standardized (e.g. LoDoPaB challenges), In future, *We can expect more reproducible comparisons*. *In summary, neural methods for LDCT continue to evolve rapidly, making low-dose, sparse-view CT increasingly viable for high-quality imaging.*

7 REFERENCES

Adler, J. and Öktem, O. (2018) 'Learned Primal-Dual Reconstruction', *IEEE Transactions on Medical Imaging*, 37(6). Available at: https://doi.org/10.1109/TMI.2018.2799231.

American Association of Physicists in Medicine (no date) *Low Dose CT Grand Challenge*.

Björck, Å. (1996) *Numerical Methods for Least Squares Problems*, *Numerical Methods for Least Squares Problems*. Available at: https://doi.org/10.1137/1.9781611971484.

Blake, G. (2020) *Low Dose CT Image and Projection Data (LDCT-and-Projection-data)*, *The Cancer Imaging Archive*.

Boyd, S. *et al.* (2010) 'Distributed optimization and statistical learning via the alternating direction method of multipliers', *Foundations and Trends in Machine Learning*. Available at: https://doi.org/10.1561/2200000016.

Chen, H., Zhang, Y., Zhang, W., *et al.* (2017) 'aLow-dose CT via convolutional neural network', *Biomedical Optics Express*, 8(2). Available at: https://doi.org/10.1364/boe.8.000679.

Chen, H., Zhang, Y., Kalra, M.K., *et al.* (2017) 'Low-Dose CT with a residual encoder-decoder convolutional neural network', *IEEE Transactions on Medical Imaging*, 36(12). Available at: https://doi.org/10.1109/TMI.2017.2715284.

Daubechies, I., Defrise, M. and De Mol, C. (2004) 'An iterative thresholding algorithm for linear inverse problems with a sparsity constraint', *Communications on Pure and Applied Mathematics*, 57(11). Available at: https://doi.org/10.1002/cpa.20042.

Deep Inversion Validation Library (Dival) (no date) *https://github.com/jleuschn/dival.git*.

Greif, C. and Wathen, M. (2019) 'Conjugate gradient for nonsingular saddle-point systems with a maximally rank-deficient leading block', *Journal of Computational and Applied*

Mathematics, 358. Available at: https://doi.org/10.1016/j.cam.2019.02.016.

Han, Y. and Ye, J.C. (2018) 'Framing U-Net via Deep Convolutional Framelets: Application to Sparse-View CT', *IEEE Transactions on Medical Imaging*, 37(6). Available at: https://doi.org/10.1109/TMI.2018.2823768.

He, J., Wang, Y. and Ma, J. (2020) 'Radon Inversion via Deep Learning', *IEEE Transactions on Medical Imaging*, 39(6). Available at: https://doi.org/10.1109/TMI.2020.2964266.

Huang, Z. *et al.* (2022) 'DU-GAN: Generative Adversarial Networks with Dual-Domain U-Net-Based Discriminators for Low-Dose CT Denoising', *IEEE Transactions on Instrumentation and Measurement*, 71. Available at: https://doi.org/10.1109/TIM.2021.3128703.

Koetzier, L.R. *et al.* (2023) 'Deep Learning Image Reconstruction for CT: Technical Principles and Clinical Prospects', *Radiology*. Available at: https://doi.org/10.1148/radiol.221257.

Landweber, L. (1951) 'An Iteration Formula for Fredholm Integral Equations of the First Kind', *American Journal of Mathematics*, 73(3). Available at: https://doi.org/10.2307/2372313.

Leuschner, J. *et al.* (2021) 'LoDoPaB-CT, a benchmark dataset for low-dose computed tomography reconstruction', *Scientific Data*, 8(1). Available at: https://doi.org/10.1038/s41597-021-00893-z.

LIDC-IDRI | A completed reference database of lung nodules on CT scans (no date) *https://doi.org/10.7937/K9/TCIA.2015.LO9QL9SX*.

Liu, T. *et al.* (2020) 'Interpreting U-Nets via Task-Driven Multiscale Dictionary Learning', *arXiv* [Preprint].

Marcos, L. *et al.* (2022) 'Dilated Convolution ResNet with Boosting Attention Modules and Combined Loss Functions for LDCT Image Denoising', in *Proceedings of the Annual International Conference of the IEEE Engineering in Medicine and Biology Society, EMBS*. Available at: https://doi.org/10.1109/EMBC48229.2022.9870993.

Natterer, F. and Wang, G. (2002) 'The Mathematics of Computerized Tomography', *Medical Physics*, 29(1). Available at: https://doi.org/10.1118/1.1429631.

Sadia, R.T., Chen, J. and Zhang, J. (2024) 'CT image denoising methods for image quality improvement and radiation dose reduction', *Journal of Applied Clinical Medical Physics*. Available at: https://doi.org/10.1002/acm2.14270.

Selig, T. *et al.* (2025) 'Enhanced Low-Dose CT Image Reconstruction by Domain and Task Shifting Gaussian Denoisers'.

Shanno, D.F. (1970) 'Conditioning of quasi-Newton methods for function minimization', *Mathematics of Computation*, 24(111). Available at: https://doi.org/10.1090/s0025-5718-1970-0274029-x.

Shepp, L.A. and Vardi, Y. (1982) 'Maximum Likelihood Reconstruction for Emission Tomography', *IEEE Transactions on Medical Imaging*, 1(2). Available at: https://doi.org/10.1109/TMI.1982.4307558.

Wang, D. *et al.* (2023) 'CTformer: convolution-free Token2Token dilated vision transformer for low-dose CT denoising', *Physics in Medicine and Biology*, 68(6). Available at: https://doi.org/10.1088/1361-6560/acc000.

Wang, H. *et al.* (2023) 'Degradation Adaption Local-to-Global Transformer for Low-Dose CT

Image Denoising', *Journal of Digital Imaging*, 36(4). Available at: https://doi.org/10.1007/s10278-023-00831-y.

Wojcik, A. (2022) 'Reflections on effects of low doses and risk inference based on the UNSCEAR 2021 report on "biological mechanisms relevant for the inference of cancer risks from low-dose and low-dose-rate radiation"', *Journal of Radiological Protection*, 42(2). Available at: https://doi.org/10.1088/1361-6498/ac591c.

Yang, Q. *et al.* (2018) 'Low-Dose CT Image Denoising Using a Generative Adversarial Network With Wasserstein Distance and Perceptual Loss', *IEEE Transactions on Medical Imaging*, 37(6). Available at: https://doi.org/10.1109/TMI.2018.2827462.

Zamir, S.W. *et al.* (2022) 'Restormer: Efficient Transformer for High-Resolution Image Restoration', in *Proceedings of the IEEE Computer Society Conference on Computer Vision and Pattern Recognition*. Available at: https://doi.org/10.1109/CVPR52688.2022.00564.

Zhang, K. *et al.* (2022) 'Plug-and-Play Image Restoration With Deep Denoiser Prior', *IEEE Transactions on Pattern Analysis and Machine Intelligence*, 44(10). Available at: https://doi.org/10.1109/TPAMI.2021.3088914.

Zhang, X. *et al.* (2024) 'Transferring U-Net between low-dose CT denoising tasks: a validation study with varied spatial resolutions', *Quantitative Imaging in Medicine and Surgery*, 14(1). Available at: https://doi.org/10.21037/qims-23-768.

Zhu, B. *et al.* (2018) 'Image reconstruction by domain-transform manifold learning', *Nature*, 555(7697). Available at: https://doi.org/10.1038/nature25988.

8 Artefact

Colab code was converted to html via; *!jupyter nbconvert mynotebook.ipynb* --to html and attached as a submission with the report + at the canvas portal to submit code. Didn't copy here due the *large no. of CT image outputs in the notebook making the word document not responding*.

Pls refer to Evaluation → All model evaluation cell to refer to the result sheet below